Forest gain across tropical and subtropical Asia masks widespread loss of complex forests

Martin Brandt

martin.brandt@mailbox.org

Københavns Universitet https://orcid.org/0000-0001-9531-1239

Xin Xu

University of Copenhagen

Xiaowei Tong

Institute of Subtropical Agriculture, Chinese Academy of Sciences, Changsha

Josep Peñuelas

CREAF-CSIC https://orcid.org/0000-0002-7215-0150

Jerome Chave

Université de Toulouse

Christian Igel

Department of Computer Science, University of Copenhagen

Philippe Ciais

CEA CNRS UVSQ, Centre d'Etudes Orme des Merisiers https://orcid.org/0000-0001-8560-4943

Jon Sporring

University of Copenhagen https://orcid.org/0000-0003-1261-6702

Sizhuo Li

Copenhagen University https://orcid.org/0000-0001-9583-7230

Maurice Mugabowindekwe

Københavns Universitet https://orcid.org/0000-0003-0803-7417

Florian Reiner

Københavns Universitet

Dimitri Gominski

University of Copenhagen https://orcid.org/0000-0002-8135-1341

Yuemin Yue

Chinese Academy of Sciences

Kelin Wang

Institute of Subtropical Agriculture, Chinese Academy of Sciences, Changsha https://orcid.org/0000-0001-8218-5368

Quie Xu

Chinese Academy of Sciences

Yongqing Bai
State Key Laboratory of Remote Sensing Science, Aerospace Information Research Institute, Chinese Academy of Sciences, Beijing 100101, China https://orcid.org/0000-0002-2169-3577
Zhengchao Chen
State Key Laboratory of Remote Sensing Science, Aerospace Information Research Institute, Chinese Academy of Sciences
Rasmus Fensholt
University of Copenhagen https://orcid.org/0000-0003-3067-4527

Biological Sciences - Article

Keywords:

Posted Date: July 29th, 2026

DOI: https://doi.org/10.21203/rs.3.rs-10077701/v1

Additional Declarations: There is **NO** Competing Interest.

Forest gain across tropical and subtropical Asia masks widespread loss of complex forests

Xin Xu[1,2], Martin Brandt[1]*, Xiaowei Tong[2]*, Josep Peñuelas[3,4], Jérôme Chave[5], Christian Igel[6,7], Philippe Ciais[8], Jon Sporring[6], Sizhuo Li[1], Maurice Mugabowindekwe[1], Florian Reiner[1], Dimitri Gominski[1], Yuemin Yue[2], Kelin Wang[2], Qiue Xu[2,9], Yongqing Bai[10], Zhengchao Chen[10], Rasmus Fensholt[1]

[1] Department of Geosciences and Natural Resource Management, University of Copenhagen, Copenhagen, Denmark
[2] Huanjiang Observation and Research Station for Karst Ecosystem, Guangxi Key Laboratory of Karst Ecological Processes and Services, Institute of Subtropical Agriculture, Chinese Academy of Sciences, Changsha 410125, China
[3] CSIC, Global Ecology Unit, CREAF-CSIC-UAB, Bellaterra, 08193 Barcelona, Catalonia, Spain
[4] CREAF, Cerdanyola del Vallès 08193, Catalonia, Spain
[5] Centre de Recherche sur la Biodiversité et l'Environnement, CNRS, IRD, INPT, Université de Toulouse, Toulouse, France
[6] Department of Computer Science, University of Copenhagen, Copenhagen, Denmark
[7] Pioneer Centre for Artificial Intelligence, Copenhagen, Denmark
[8] Laboratoire des Sciences du Climat et de l'Environnement, CEA/CNRS/UVSQ/Université Paris Saclay, Gif-sur-Yvette, France
[9] University of Chinese Academy of Sciences, Beijing 100049, China
[10] State Key Laboratory of Remote Sensing Science, Aerospace Information Research Institute, Chinese Academy of Sciences, Beijing 100101, China

Abstract

Forest cover has expanded across tropical and subtropical Asia in recent decades, but area alone is an inadequate metric because it does not capture forest structure, which is critical for supporting key ecosystem functions and services, including biodiversity. Here, we apply sub-meter resolution satellite imagery to characterize the complexity of forests from a horizontal perspective by quantifying the diversity of tree crown sizes and their spatial arrangement across India, Southeast Asia, and southern China. We reveal large mismatches between reported forest area and the complexity of the forests. While overall, the majority of the forests still have a relatively high complexity, a recent change towards low complexity forests is observed. India, despite its large forest extent, shows a particularly low forest complexity, with more than half of its forests classified as low-complexity. Analysing forests affected by gain or loss in area between 2000 and 2024, we find that approximately three quarters of newly established forests are of low structural complexity, while high-complexity forests, concentrated in Myanmar, Laos, Cambodia, and Indonesia, continue to disappear. Our results highlight the need to move beyond forest cover statistics toward quality-based indicators for monitoring in the support of conservation policy.

Introduction

Forests are a fundamental component of the global carbon cycle, and provide essential ecosystem services[1,2]. Forest disturbance regimes have become more dynamic globally due to increased land-cover change and human management[3]. This is particularly the case for tropical and sub-tropical Asia, including India, Southern China and South East Asia, where both deforestation and reforestation/afforestation are widespread, driven by a range of factors, such as wood demand, agricultural expansion, and ecological restoration initiatives[4-7]. In recent years, official statistics from many Asian countries have reported an annual increase in forest cover[8], which is often regarded as a key pathway for enhancing carbon sequestration and achieving carbon neutrality aims[9]. However, forest cover is a necessary but not a sufficient indicator for comprehensive forest monitoring, as ecosystem services vary substantially among different forest types[2,10-11]. In particular, intensively managed forests often maximize timber production at the cost of biodiversity and other ecological functions through practices such as monoculture plantations, short rotation cycles, and fertilization practices[12-13]. Therefore, an in-depth understanding of forest dynamics requires moving beyond simple measures of tree presence, absence, or regrowth, toward more comprehensive and quantitative indicators that capture forest quality and functional attributes.

Earth observation satellite systems can be used to track forests, their cover, canopy height and biomass[14-16], but it is often unclear to what extent newly established forest results from natural regeneration or human intervention[17-18]. Distinguishing new forest types is critical, because ecosystem services depend on forest naturalness and diversity[19-20], and a regularly harvested monoculture plantation may cause more environmental harm than benefit[21]. Maps exist that classify management types, such as oil palm plantations[22], natural versus planted forests[23], and distinguishing natural from modified habitats[24]. While these discrete classes are important for forest-level characterization, they are unable to capture continuous spatial variations in the complexity of a forest. For example, a newly planted or regenerating forest is not necessarily a monoculture and can feature a high species diversity[25]. Assessing the true diversity of a forest requires continuous and spatially explicit indicators rather than discrete classes used at forest stand-level, thereby supporting more refined monitoring and sustainable management strategies.

Forest structure is a critical indicator for characterizing forest diversity and ecological functioning[26,27]. By linking observable structural traits to ecosystem processes, structure provides a quantitatively measurable metric for capturing the continuous variation of ecosystem services[28-29]. LiDAR enables the characterization of forest structural attributes by penetrating multiple canopy layers to capture detailed vertical profiles[30], from which quantitative indicators reflecting structural heterogeneity, such as foliage height diversity and vertical distribution ratio[31-32], can be derived, thereby providing comprehensive insights into vertical forest structural complexity. In theory, the complexity of forest structure can serve as a proxy for forest naturalness[33]. Generally, naturally regenerated forests typically exhibit multi-layered canopies, heterogeneous stand structures and diverse species composition, whereas monoculture plantations, due to fixed planting schedules, limited species selection and economic-driven management often display simpler and more homogeneous structures[34]. However, airborne LiDAR is not available over large areas as studied here, and spaceborne lidar has a relatively coarse spatial resolution[28], with ~25 m GEDI footprints often

capturing mixed vegetation conditions, limiting its use in characterizing the complexity of the spatial interrelationship between trees. High resolution optical images allow us to assess trees as single objects, and studying how individual trees are spatially distributed in relation to each other has recently been used to characterize the complexity of forests from an horizontal perspective[35]. Here, we characterize the horizontal structural complexity (HSI) by quantifying the diversity of tree crown sizes and their spatial arrangement. HSI serves as a sensitive indicator of niche availability and resource competition. High variance in crown sizes and irregular spatial packing reflect a history of natural gap dynamics and multi-age recruitment, which are the hallmarks of high-biodiversity ecosystems. In contrast, the spatial 'grid-locking' of crowns in low-HSI areas indicates a suppression of natural successional processes, resulting in a more vulnerable and 'leaky' carbon-nutrient cycle[36].

We developed a continuous index of horizontal forest complexity based on sub-meter resolution GaoFen-2 and 3-m PlanetScope satellite imagery across India, Southeast Asia, and southern China. The index captures the diversity of tree crown sizes and their spatial arrangement around the year 2020. We tested whether this satellite-derived measure of crown structure spatial variability can serve as an indicator to reflect forest naturalness, and mapped where high-complexity forests are being found, and where they are lost. Furthermore, we assessed where newly established forests are recovering structural complexity and where they remain structurally simple.

Results

An index to reflect the naturalness of forests

To restrict our analyses to forested areas, we first trained a tree detection model able to map trees inside and outside forests at 3-m resolution from PlanetScope (see Methods). To assess the forest complexity within this mask, we segmented individual tree crowns in more than 100,000 km^2 of sub-meter GaoFen-2 imagery (Extended Data Figs. 1,2) and extracted tree locations and crown size variables. The diversity of tree crown sizes among neighbouring trees and Ripley's K function[37-39] was then used to generate the horizontal structure index (HSI) for trees within 100x100 m grids (Extended Data Fig. 3). Higher HSI values correspond to greater variability in crown size and increased spatial heterogeneity in overstory tree distribution within the 100 m grids. This was used to train a second model based on PlanetScope imagery, covering approximately 98 million km² cumulatively across years, to produce wall-to-wall maps of HSI across the entire study area (see Extended Data Fig. 4a for model accuracies). The HSI showed relationships with existing forest structure variables, such as the vertical structure (WSCI – Waveform Structural Complexity Index)[30], aboveground biomass[40], forest intactness[41] and biodiversity intactness[42] (Fig. 1b, Extended Data Fig. 5), supporting that this index successfully encapsulates the variability in forest structure.

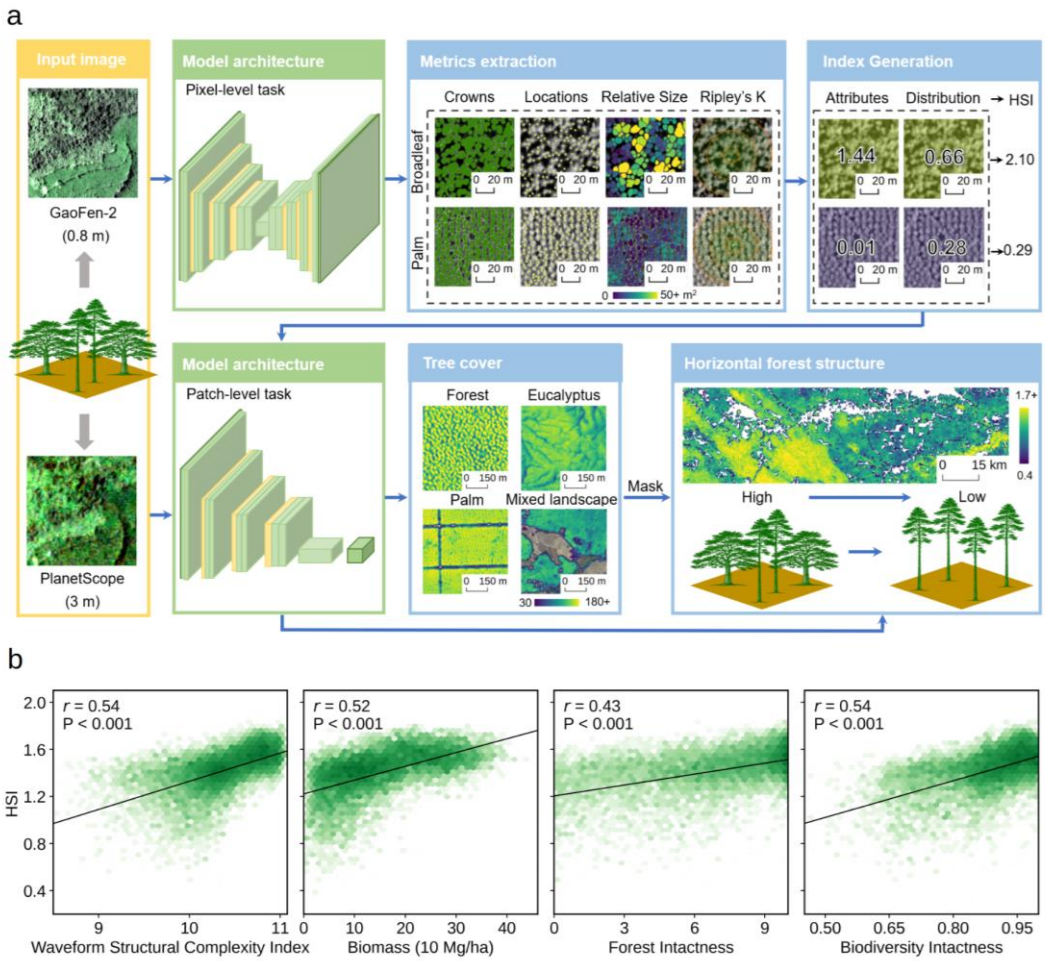

Figure 1: Developing an index capturing the horizontal forest structure complexity. a, *Workflow for mapping horizontal forest structure complexity index (HSI). Two wall-to-wall products were generated: (i), tree detection heatmap, and (ii), forest structure complexity map.* ***b,*** *Relationships between HSI and vertical structure derived from GEDI[30], aboveground biomass[40], forest Intactness[41], and biodiversity Intactness[42].The darker colors indicating higher densities. To ensure that our HSI was not confounded by varying stem densities, we performed partial correlation analyses between HSI and other structural variables. We found that the structural complexity signal remained significant ($p < 0.001$) even after controlling for tree density[43]. This confirms that HSI captures the functional architecture of the canopy, the relative arrangement and size-diversity of trees, rather than just the density of individuals detected by the sensors.*

Using existing data on forest management[44], we show that HSI decreases with increasing management intensity (Fig. 2f). For example, the class "*naturally regenerating forest without management*" exhibits the highest HSI (mean = 1.53, s.d. = 0.16), followed by "*naturally regenerating forest with management*" (mean =1.40, s.d. = 0.19). Planted forests and plantation forests showed an even lower HSI (mean = 1.36, s.d. = 0.19); while oil palm plantations exhibited the lowest HSI (mean = 1.15, s.d. = 0.23). Agroforestry characterized by mixed landscapes displayed intermediate complexity with greater variability (mean = 1.34, s.d. = 0.23). Moreover, HSI varies across different habitat states[24] (Fig. 2g): Highest values are found in "*likely natural habitats*" (mean =1.49, s.d. = 0.19), followed by "*potential natural habitats*" (mean = 1.41, s.d. = 0.20), and lower values are observed in both "potential modified

habitats" (mean = 1.10, s.d. = 0.29) and "likely modified habitats" (mean = 0.95, s.d. = 0.33). The standard errors of the mean (SEM) were small across all management and habitat groups, ranging from 0.24 × 10^{-4} to 0.27 × 10^{-3}. Similarly, forests within protected areas had higher structural complexity values than those outside protected areas (Fig. 2h). While none of the applied datasets provide a high level of detail, the convergence of patterns gives confidence that HSI can be used to reflect the impact of management on the structural complexity of forests.

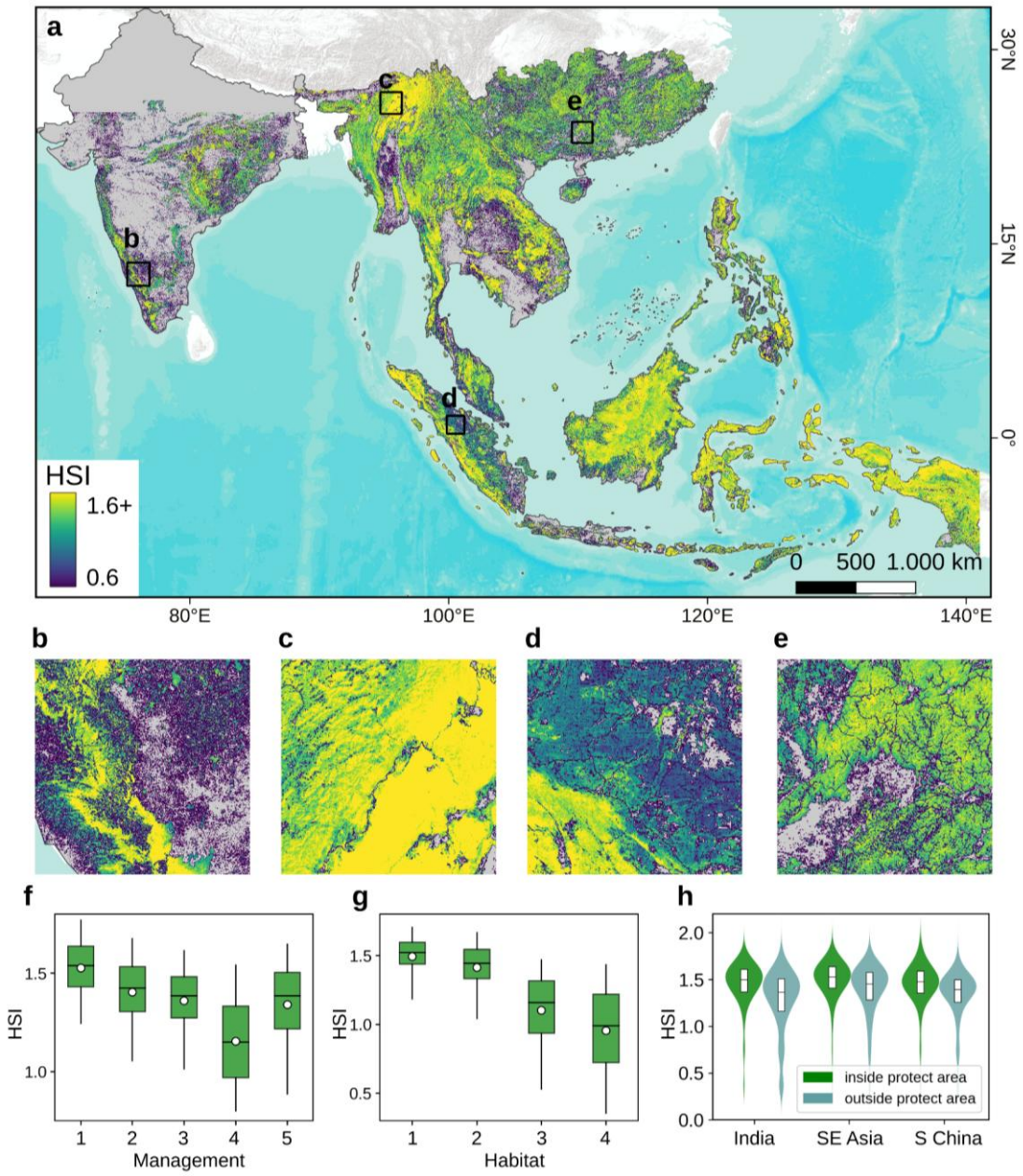

***Figure 2: Horizontal forest structural complexity (HSI) across management types. a**, Spatial patterns of HSI across forest areas aggregated to 500 m resolution for visualization purposes. **b-e**, Zoom in examples of HSI patterns in selected regions. **f**, HSI distributions across different forest management intensities, including naturally regenerating forest without management (Management 1), naturally regenerating forest with management (Management 2), planted and plantation forests (Management 3), oil palm plantations (Management 4), and*

agroforestry systems (Management 5)[44]. In the boxplots, the dots indicate mean HSI values. ***g****, HSI distributions across different natural and modified forest habitats, including likely natural habitat (Habitat 1), potential natural (Habitat 2), potential modified (Habitat 3) and likely modified (Habitat 4)[24]. In the boxplots, the dots indicate mean HSI values.* ***h****, violin plot of HSI inside and outside protected area in India, Southeast Asia, and Southern China.*

Forests of high and low complexity are balanced

Using existing forest type maps[45-46], we show that HSI is clearly different between primary forests and plantations (Fig. 3b). In plantations, approximately 70% of the grids have HSI values below 1.37, whereas in primary forests, 70% of grids have HSI values exceeding 1.47, reflecting the more heterogeneously spaced tree size composition and spatial arrangement of primary forests compared with the uniform structure of plantations. Based on this distribution, we categorized HSI values into three levels—high, medium, and low—for subsequent analyses.

Overall, the region's forests show a balanced picture of HSI classes, with 42% being classified as highly complex, 39% having a low complexity, and 19% in between (Fig. 3c). This distribution, however, varies between countries, and structural complexity is not proportional to reported forest area[47]. For example, India reported 72.31 million ha of forest in 2020 [47] but only 30% is classified as having a high complexity in our map. In contrast, the forest areas of Indonesia, Myanmar, and Laos exhibit substantially larger proportions of high-complexity forests, accounting for 52%, 48%, and 49% of their forest areas, respectively.

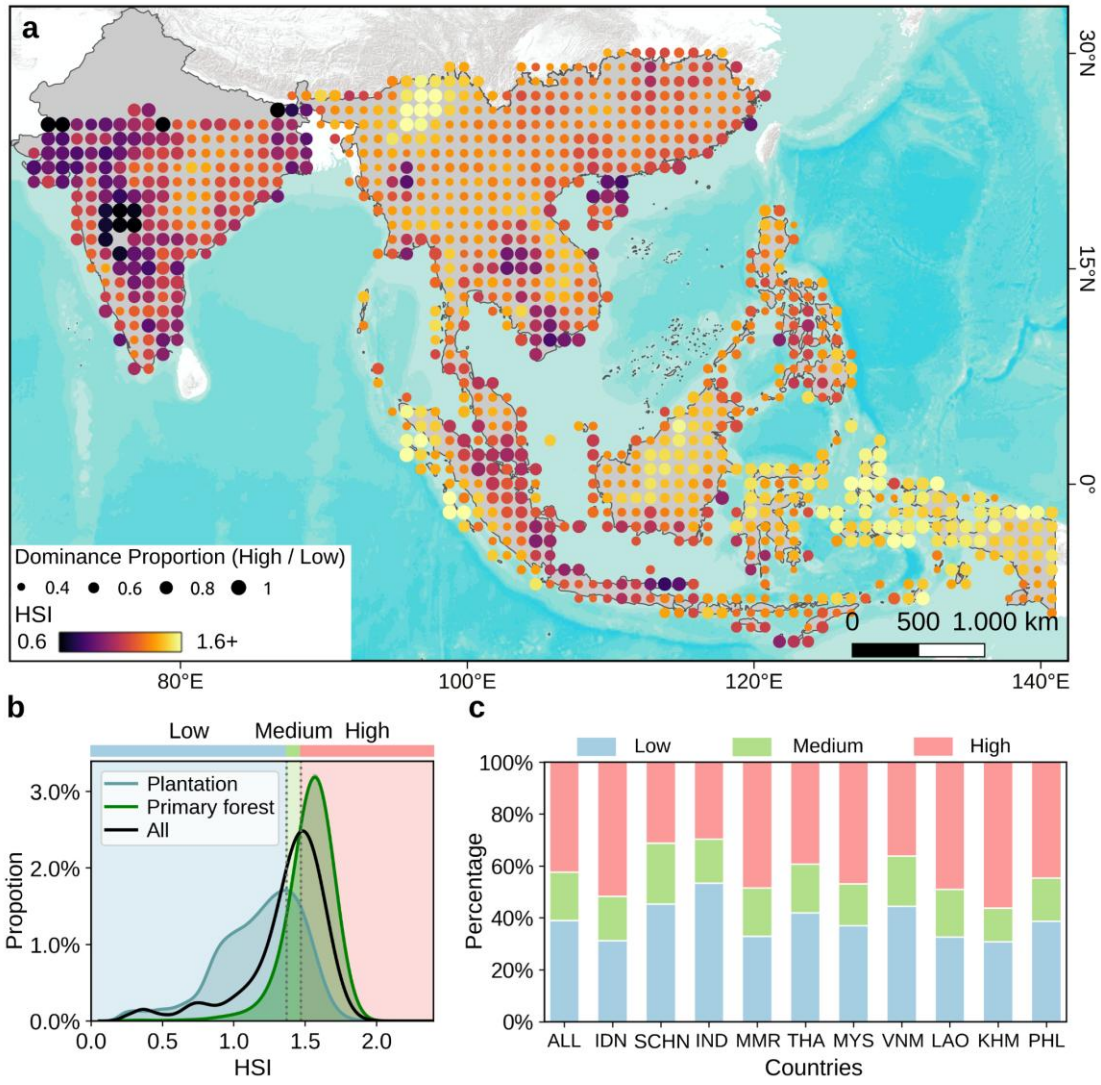

***Figure 3: Detection of high and low complexity forests. a**, Mean HSI and dominance class proportions for 1° × 1° grids. Circle color and circle size represents the mean HSI and the proportion of the dominant class (high or low). **b**, Distribution of HSI in primary forests and plantations[45-46], **c**, Proportions of high-, medium-, and low-complexity forests for the ten countries in the study area with the largest reported forest areas[47].*

Continued loss of high complexity forests

To understand the complexity of lost and newly grown forests, we used Global Forest Watch (GFW) forest loss data[48]. Since our data is static reflecting the years around 2020, we looked at the complexity of forests that were lost after 2019 to locate and quantify the loss of high diversity forests. We aggregated forest loss to match the HSI resolution and focused on grids with >75% forest loss (Fig. 4) (50% and 90% thresholds were also tested, see Extended Data Fig. 6). The results show that out of a total forest loss of 49,000 km^2, 28% of the forests had a high and 53% a low complexity. Forest loss with high structural complexity was primarily concentrated in northern Myanmar and southern Laos (Fig. 4b), as well as in tropical natural forest regions of Indonesia and Malaysia. In contrast, areas of forest loss with low structural complexity are predominantly found in plantation-dominated landscapes in Indonesia and Malaysia (Fig. 4c), and may reflect harvest. The normal distribution of HSI values of lost forests fall between plantations and primary forests (Fig. 4d), suggesting that forest loss occurs in

both plantations and natural forests. Moreover, we quantified the proportions of high-, medium-, and low-complexity classes within lost forest across countries (Fig. 4e). The results show that most forests lost in Thailand had a very low horizontal complexity (76%). Vietnam and Malaysia also show relatively high proportions of low-complexity forest loss, at 70% and 66%, respectively. In contrast, 56% of the forests lost in Cambodia show the highest structural complexity, followed by Laos (44%) and the Philippines (45%).

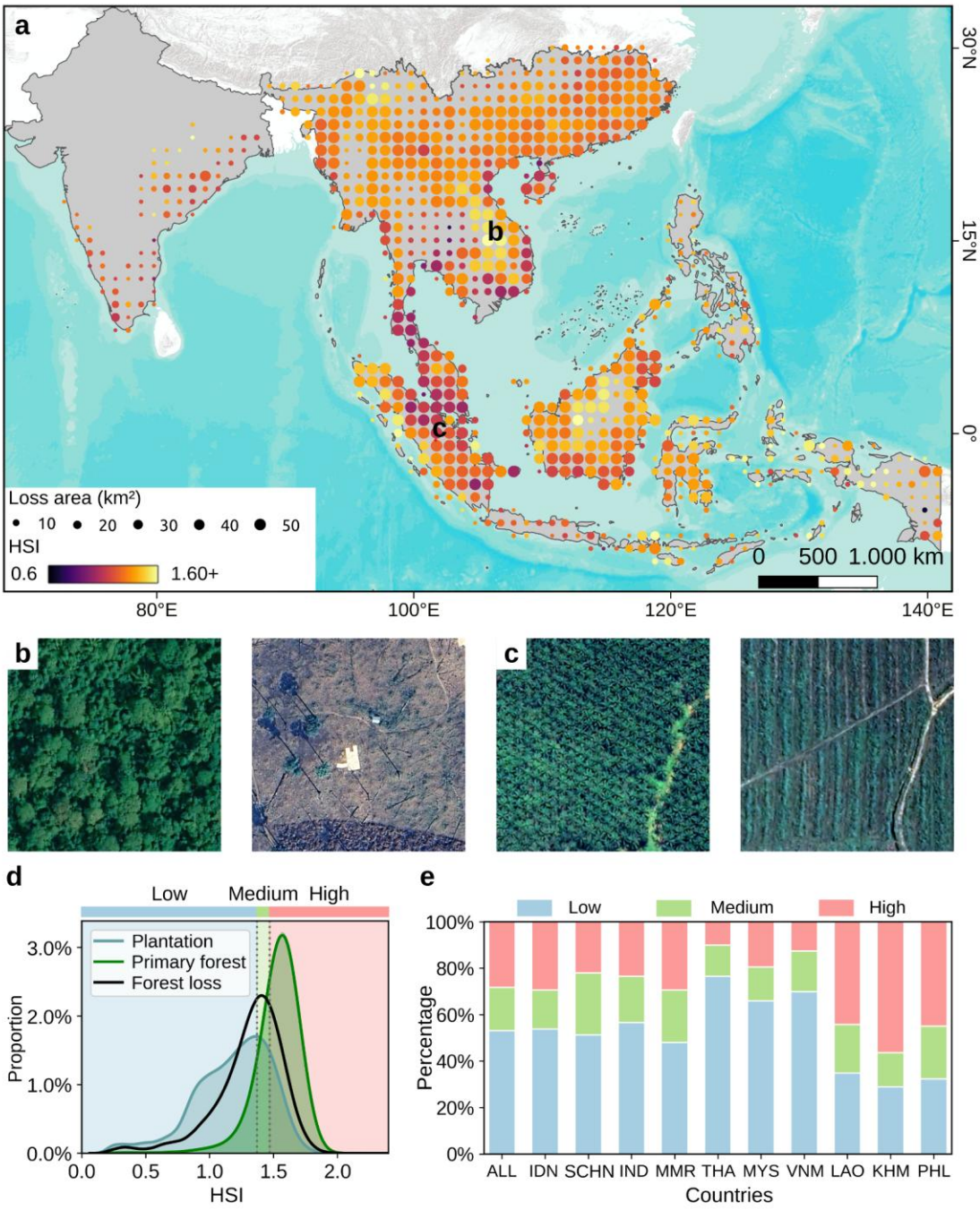

***Fig. 4 Structural complexity of forests lost after 2019**. **a,** Mean HSI and area of forest loss for 1° by 1° grids. Circle color and circle size represents the mean HSI and the loss area. **b**, Example of high-complexity forest loss between 2020 and 2025 from Google Maps satellite imagery. HSI=1.75. **c**, Example of low-complexity forest loss between 2018 and 2021 from Google Maps satellite imagery. HSI=1.10. **d,** HSI distributions of forest loss overlaid by the*

distribution of HSI in primary forests and plantations for the study area. **e***, Proportions of high-, medium-, and low-complexity of lost forests for different countries in the study area.*

Three quarters of new forests exhibit low structural complexity

Since our analysis is based on observations collected around 2020, we used forest loss data from 2000-2018 to study the complexity of newly established forests that have followed forest loss. We found that 69% of the areas mapped as forest loss during 2000-2018 showed forests in our high resolution map, implying regrowth has happened on 428,000 km^2.

We then overlaid our HSI data with areas of forest gain to assess the structural characteristics of newly established forests (Fig. 5, Extended Data Figs. 7, 8). The results indicate that the HSI density distribution of these new forests is comparable to the HSI value distribution for plantation forests (see Fig. 3b and Fig. 5d). The distribution of HSI in newly established forest areas shows a strong left-skewed distribution, with most values falling within the range of low complexity forests. This pattern did not change when using the GFW forest gain dataset[49], which may be less detailed but includes forest expansion areas (Extended Data Fig. 8). A higher complexity in new forests is primarily observed in mountainous forest areas and tropical forest regions (Fig. 5b). Medium-complexity forests account for approximately 13% of the new forests, whereas 11% showed a high complexity, and the remaining 76% had a low complexity across countries (Fig. 5e). Results show that Cambodia exhibits the lowest horizontal structural complexity in new forests, with low-complexity forests accounting for 82% and high-complexity forests comprising 9%. In contrast, the Philippines shows the highest proportion of high-complexity forests among new forests (32%).

Notably, the extreme left-skewed distribution of HSI in newly established forests (Fig. 5d) suggests a 'successional ceiling' rather than being a sign of uniformity due to the young age of trees. While naturally regenerating secondary forests typically develop horizontal heterogeneity within the first two decades via gap dynamics, the established new forests across Asia show a structural signature nearly identical to industrial monocultures. This indicates that current 'forest gain' is functionally locked into a structurally simple state that precludes the development of mature-forest niches.

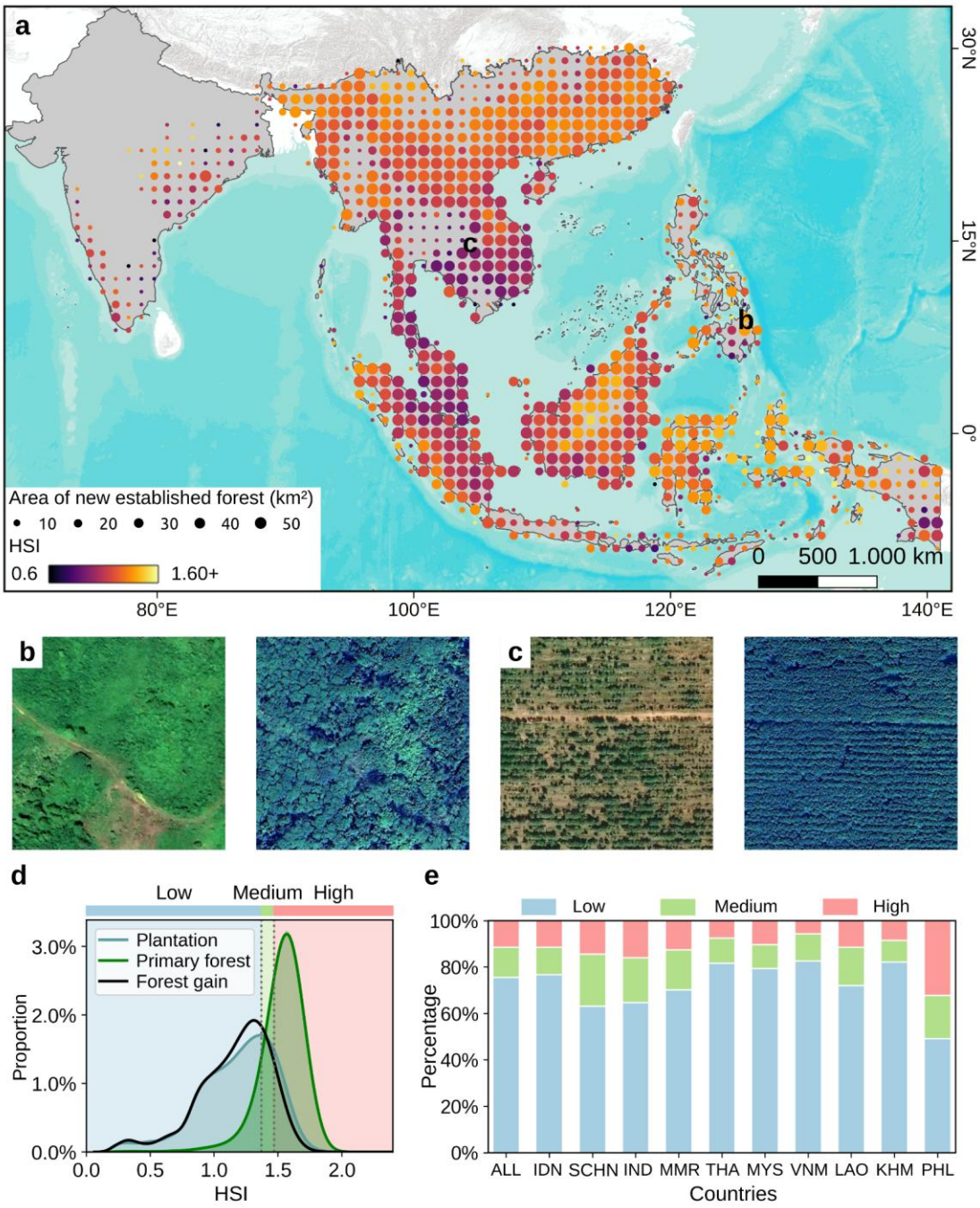

Fig. 5 Structural complexity of newly established forests since 2000. ***a***, *Mean HSI and area of new forest for 1° by 1° grids. Circle color and circle size represents the mean HSI and the area of the new forest.* ***b***, *Example of high-complexity forest gain between 2017 and 2024 from Google Maps satellite imagery. HSI=1.33.* ***c***, *Example of low-complexity forest gain between 2019 and 2024 from Google Maps satellite imagery. HSI=0.75. The HSI values observed in the examples of young plantations and young naturally regenerating secondary forests indicate that, even in early successional stages, naturally regenerating stands exhibited higher horizontal heterogeneity than plantations of comparable age, confirming that HSI effectively captures the 'management footprint' independently of forest maturity.* ***d,*** *HSI distributions of new established forests overlaid by the distribution of HSI in primary forests and plantations for the study area.* ***e***, *Proportions of high-, medium-, and low-complexity for new established forests for different countries in the study area.*

Discussion

Existing national-scale forest reports, such as the forest resources assessments from FAO, primarily rely on forest area as a core indicator, and many countries in tropical and subtropical Asia have reported a continuous increase in forest area over recent decades (Extended Data Table 1). Our study shows that forest cover expansion does not equate to forest structural complexity restoration. Currently, the distribution of low and high complexity forests in the region is still fairly balanced, but the development shows that a considerable proportion of the forests lost (after 2019) had a high complexity, while most newly established forests (during 2000-2018) have a low complexity. This indicates that mature secondary or primary forests are replaced by monoculture plantations. While this potentially maintains or increases total forest area, it is often accompanied by a decline in structural complexity. Current reporting schemes often emphasize on forest area, which is problematic, as it conceals the ongoing loss of high structural complexity natural forests at the expense of a general development towards low complexity forests[50-51]. This has implications, because forests with different structural complexities exhibit differences in ecosystem functions such as carbon storage, habitat quality, and biodiversity[27,29,34]. Therefore, a one-dimensional characterization of forest dynamics solely based on area changes may overlook essential dimensions of ecological quality[10], potentially leading to systematic overestimation of ecological recovery and masking underlying declines in ecosystem functioning.

From an ecosystem functioning perspective, the transition from high-complexity to homogenous forests implies a large-scale shift in the stoichiometry of the Asian land sink. Homogenous plantations, often characterized by high N-inputs and P-limitations, reach 'biogeochemical saturation' much faster than structurally diverse natural forests[36,52-53]. A systemic homogenization represents a critical 'biogeochemical trap'; while newly established low-complexity forests may contribute to short-term 'greening' targets, they lack the multi-layered functional niches required to sustain long-term soil carbon sequestration and climate resilience[54-55], potentially leading to earlier carbon-sink saturation across the continent. This 'functional browning', where forest area expands but structural and metabolic diversity declines, suggests that Asia's role as a reliable terrestrial carbon sink is increasingly precarious and may be systematically overestimated in models that rely solely on leaf area index or forest cover.

This issue is also reflected in biodiversity. As an important indicator of forest ecosystem functioning, biodiversity is inherently multidimensional, encompassing species composition, community structure, as well as microbial and fungal diversity[56-58]. However, different species assemblages often have a contrasted response to environmental changes, making it difficult to characterize biodiversity dynamics using a single variable[59-60]. Therefore, developing a quantifiable and ecologically more meaningful indicator is essential for understanding the relationship between forest characteristics and biodiversity, which remains a key challenge in current research[61-62].

This study contributes to addressing the need for characterizing forests beyond traditional area-based variables. Our maps are based on sub-meter resolution images obtained by commercial sensors, and therefore our approach is only amenable to operational use globally,

upon access to representative sample areas of similar imagery for other tropical forest areas in Africa as well as Central and South America. Moreover, the horizontal perspective limited to the upper canopies cannot characterize the full range of ecological functions, but our approach makes full use of state-of-the-art data and methods to reveal patterns clearly related to the management aspect. Compared to existing forest structure frameworks that primarily rely on vertical structural metrics, this study focuses on the horizontal perspective, emphasizing tree spatial arrangement and attribute heterogeneity in forest structure quantification. By relying on relatively simple and observable variables, such as distance between tree crowns, crown size differences, and their spatial arrangement, our data establishes a link between measurable spatial information and underlying ecological processes, while offering scalability and applicability towards large-scale studies. The forest structural complexity index proposed in this study provides an operational framework that complements traditional vertical and area-based indicators, and reveals patterns that are not visible from previous indices focusing on the vertical structure (Extended Data Fig 9.). Although the relationships between forest structure and biodiversity require further investigation, this study provides a foundation for their quantitative analysis and promotes more comprehensive forest ecosystem assessment. Ultimately, our study highlights the rise of 'paper-forests' across Asia, landscapes that satisfy international reporting requirements for forest expansion but fail to deliver the biodiversity of the systems they replace. Moving forward, global restoration targets (e.g., the Bonn Challenge or Kunming-Montreal Framework) must mandate the reporting of structural complexity metrics alongside forest area. Only by measuring the functional architecture of our forests can we prevent the 'invisible' degradation of the world's most critical terrestrial carbon-water-biodiversity nexus.

Methods

Overview

Our approach capitalizes on the detectability of individual trees as objects in high-resolution optical imagery. If these objects can be singled out, their spatial distribution and heterogeneity of their attributes (such as crown sizes) can be directly measured and related to real-world variables, such as management types, species diversity, etc. In summary, our work integrates optical imagery and deep learning approaches to characterize forest horizontal structural complexity for India, Southeast Asia and southern China (Fig. 1). First, sub-meter imagery from Gaofen-2 and Gaofen-7 and 105,000 manually annotated tree crown labels were used to train a deep learning model for individual tree crown segmentation, from which tree crown size and tree location are subsequently extracted. This was used to characterize the spatial patterns of individual trees and their neighbors. These spatial metrics are further aggregated at the grid scale to develop the complexity index reflecting the horizontal forest structure (HSI).

Since sub-meter imagery was not available for the entire study area, the HSI derived from sub-meter imagery was then used to train PlanetScope imagery (3-m resolution) in a second deep learning model resulting in a wall-to-wall mapping of HSI. To constrain the analysis to forest areas, a high-resolution tree confidence map was generated based on PlanetScope imagery. The predicted HSI map was masked to exclude non-forested regions using the tree confidence map and also settlement footprint data[63].

Satellite imagery

We used Gaofen-2 imagery acquired between 2017 and 2024 for individual tree crown segmentation. The data include red, green, blue, and near-infrared bands, equipped with a 0.8 m panchromatic band and 3.2 m multispectral bands. For areas with missing data, Gaofen-7 imagery was used, with 0.65 m panchromatic data resampled to 0.8 m. All Gaofen images were processed through an automated workflow, including radiometric enhancement, orthorectification, pan-sharpening, image registration and standardized tiling. After processing, we obtained 937 Gaofen images with a spatial resolution of 0.8 × 0.8 m, covering about 100,000 km2 (Extended Data Fig. 1). The workflow is described in detail in ref [64].

We used PlanetScope imagery for wall-to-wall mapping of HSI and tree cover. The dataset includes red, green, blue, and near-infrared bands at a spatial resolution of 3 m. We followed the downloading workflow described in ref [65] and ref [66]. The framework uses MODIS phenology data to select a period where trees have full leaves, and ranks all available images within 1° × 1° degrees according to their meta-data. The 1° × 1° degree tile is then filled with images having the highest quality according to the meta-data fields “clear percent”, “clear confidence”, and “visible confidence”. All images were reprojected to the WGS84 coordinate system. Histogram matching was applied to each downloaded scene using Sentinel-2 composites from 2018 to 2020 to reduce spectral and color inconsistencies before the 1° × 1° mosaics were constructed. We generated mosaics from approximately 13,000 PlanetScope images around the year 2020. We tested predictions on annual mosaics but found that the majority of the changes between years were rather related to image quality differences than real changes, so we averaged results over all available images to generate a static but robust map approximately representing the year 2020.

Tree crown segmentation using Gaofen images

We manually annotated tree crowns in GF-2 images across different land use types using QGIS 3.22. The dataset was based on the labels provided by ref. [36] (79, 838 labels), and extended to a total of 105,000 tree crown samples across the study area, of which 80% were used for training and 20% for validation. We used a U-Net architecture for tree crown segmentation as described in ref. [67]. This framework has been widely applied to tree segmentation tasks at different scales, and details can be found in ref. [14], ref. [68] and ref. [69]. Our model was trained using an input patch size of 256 × 256 pixels and a batch size of 16. We used the Tversky loss function[70] with $\alpha = 0.5$ and $\beta = 0.5$ to handle potential class imbalances. To better preserve the details of the manually labeled data, the GF-2 imagery was resampled from 0.8 m to 0.4 m resolution for both training and prediction. To separate clustered crowns in dense forest, we applied the post-processing approach proposed by ref. [68], which assumes tree crowns are approximately round and relabels the crown center through weighted distance calculation. Both the deep learning and post-processing workflows were implemented in Python 3.8. Model accuracy was evaluated based on an independent test set following ref. [36]. We refer to previous applications [36] for details, considering the similarity in both methodology and study area.

Tree cover from PlanetScope images

We generated tree cover maps from PlanetScope to mask out non-forest areas. The tree detection framework was established using PlanetScope imagery for India in ref. [66]. The framework uses point labels to detect trees or groups of trees as objects. While the original

model was solely based on about 300,000 manual point labels, here we expanded for the entire study area by training the model with tree crown centers from GaoFen imagery (about 5 million), including all forested and non-forested landscapes. The expansion did not change the accuracy metrics from the original model (F1 score of 0.65). Details of the method can be found in ref. [66]. During model training, discrete tree center labels were converted into continuous Gaussian kernels. The default scale of the Gaussian is controlled by the hyperparameters sigma (here set to 4 m) and delta (here set to 0.2), and is continuously adapted during training with a dynamic scale map. The model was trained using multi-temporal PlanetScope imagery around the year 2020. In contrast to ref. [66], we did not convert the predictions to points and did not identify trees as individuals, but used the confidence heatmap as a reflection of tree cover at a high level of detail. We tested annual mosaics, but found that changes are largely driven by inconsistencies and quality variability in PlanetScope imagery, so we further applied a percentile-based (75th) aggregation over multiple images to derive a stable static tree distribution map. As a final step, following ref. [66], pixels with confidence values higher than 0.35 were classified as tree and below as no-tree, resulting in a 3-m resolution binary map.

Horizontal forest structure index (HSI) from Gaofen images

Forest structure complexity from a horizontal perspective primarily refers to the spatial configuration of trees and the heterogeneity of their attributes [28]. It is closely related to factors such as tree species composition and stand age structure [27,71], and plays an essential role in influencing ecosystem functions and services [27]. Generally, forest stands with more heterogeneous spatial arrangements and greater variability in individual attributes tend to exhibit higher structural complexity [27-28], which is often linked to enhanced ecological benefits. They can still provide insights into competitive interactions and related ecological processes, thereby serving as informative indicators of forest structural characteristics [72]. Remote sensing data enable the acquisition of continuous spatial information across large spatial extents, thereby providing essential support for the regional-scale quantification of forest structural complexity.

At the field plot scale, structural complexity, characterized by variation in tree attributes and spatial pattern, has been widely applied [73-74]. The development of individual tree segmentation techniques from remote sensing imagery provides a foundation for scaling these approaches to larger spatial extents [65,67-68]. This study builds on this by characterizing forest structural metrics at the individual tree level based on tree segmentation results, here including two key dimensions: “tree attribute heterogeneity” and “spatial distribution pattern”. Specifically, we extracted the crown size and location of individual trees from canopy segmentation results to quantify the spatial relationships between individual trees and their neighbors. These tree-level metrics were subsequently aggregated to the grid scale to construct the Horizontal Structure Index (HSI), thereby enabling the assessment of forest structural complexity at the regional scale.

The crown size derived from individual tree segmentation was used as a representative variable to characterize the structural features of individual trees. Crown size is strongly corrected with tree height, stem diameter, and biomass [75], and can be readily extracted from satellite images. To quantify the heterogeneity of crown sizes, we considered a circular area with a diameter of 20 m around each tree. Let the set $B_{20}(k)$ contain all the trees within a

distance of 20 m from tree k. The crown size variability x_k of tree k was computed as

$$x_k = \sqrt{\frac{1}{|B_{20}(k)|}\sum_{j\in B_{20}(k)}\left(C_j - \overline{C_k}\right)^2}$$

with C_j being the crown size of tree j derived from the segmentation and $\overline{C_k} = \frac{1}{|B_{20}(k)|}\sum_{j\in B_{20}(k)} C_j$ being the mean crown size within the circular plot.

These tree-level metrics were subsequently aggregated at the level of 100×100 m^2 grid cells. Let the set T_c contain the trees in grid cell c and $\bar{x}_c = \frac{1}{|T_c|}\sum_{j\in T_c} x_j$ be the mean crown variability in that cell. Then we defined the coefficient of variation CV_c in cell c as

$$\mathrm{CV}_c = \frac{1}{\bar{x}_c}\sqrt{\frac{\sum_{j\in T_c}\left(x_j - \bar{x}_c\right)^2}{|T_c|}}$$

Furthermore, we computed the weighted standard deviation SD_c^w per cell

$$\mathrm{SD}_c^w = \sqrt{\frac{\sum_{j\in T_c} w_j\left(x_j - \bar{x}_c^w\right)^2}{\sum_{j\in T_c} w_j}}$$

The weights were given by the canopy cover

$$w_j = \frac{\sum_{k\in S_{100}(j)} C_k}{1\mathrm{ha}}$$

where $S_{100}(j)$ are the trees within a one-hectare square area centered at tree j and $\bar{x}_c^w = \frac{\sum_{k\in T_c} w_k x_k}{\sum_{k\in T_c} w_k}$ is the weighted mean. That is, SD_c^w puts more weight on trees surrounded by an area of dense canopy cover.

We study the spatial distribution of the trees using Ripley's K-function[37-39]. Ripley's K function $K(r)$ is the expected number of other trees within distance r of an arbitrary tree divided by the average density of trees, often estimated as the number of trees per unit area. It allows us to analyze tree spatial patterns independent of tree density by comparing the deviation between the observed point pattern and a completely random distribution at different spatial scales. In this study, Ripley's K-function is calculated across multiple distance scales r, with 20 evenly spaced distances between 0 and 40 m. Principal Component Analysis is applied at the grid scale to extract the most representative component of the function $K(r)$ characterizing tree spatial distribution.

We then integrated individual tree attribute variability, represented by crown size, with the spatial pattern metrics derived from Ripley's K-function. The two components were normalized and summed to generate the horizontal structure index (HSI) at the grid scale, providing a comprehensive representation of the horizontal complexity of forests.

Horizontal forest structure index (HSI) from PlanetScope images

The Gaofen based results are highly detailed but difficult to scale. High quality sub-meter images are typically not available over large areas, and in particular tropical areas are poorly covered due to persistent cloud cover. PlanetScope is the only sensor that provides global high resolution imagery at an almost daily frequency. However, the 3-m resolution makes it

challenging to segment individual trees, particularly in younger forests, where tree crowns are small. Consequently, we did not apply the same framework as we applied on Gaofen images to PlanetScope images, but we used the HSI results based on Gaofen to train a deep learning patch-level regression model. The idea is that the model sees the PlanetScope image for a specific patch, and knows the corresponding HSI value for this patch, and this information can then be used to infer HSI for similar patches only from PlanetScope images. Specifically, the HSI derived from high-resolution Gaofen imagery was used as the training label, whereas multispectral PlanetScope imagery with red, green, blue, and near-infrared bands was used as the model input. The model was trained on 32 × 32 3-m pixel patches to capture both spatial texture characteristics and spectral information. The model adopts a convolutional neural network (CNN)-based architecture, with the backbone initialized using weights pre-trained on ImageNet. The model input was standardized before training. Features were extracted through multiple convolutional layers, with the spatial resolution of the feature maps gradually decreasing and the number of channels increasing within the encoder[76]. Global average pooling, followed by three fully connected layers, is then applied to gradually reduce the feature dimensionality to a single value corresponding to the HSI of the target patch. To characterize the uncertainty of the model's predictions, we used Gaussian Negative Log-Likelihood (NLL) as the loss function, enabling the model to estimate HSI values and their associated uncertainties while optimizing prediction accuracy. Due to variability in the quality of PlanetScope imagery, time-series HSI predictions were integrated at 200m resolution. For model evaluation, 269 patches are randomly selected to construct an independent test set, which is excluded from all stages of model training and parameter tuning to ensure the independence of evaluation. Root Mean Square Error (RMSE) and bias are used as evaluation metrics to quantitatively evaluate the model’s prediction performance. On the independent test dataset, the RMSE was 38.16%, with an overall overestimation bias of 11.93% (Extended Data Fig. 4).

Data availability

The Gaofen satellite images used for this study are commercial data and cannot be distributed at this point. Derived products, such as the horizontal structure index, tree cover maps, will be made available upon acceptance of the manuscript. GEDI L4C Global Waveform Structural Complexity Index (WSCI) Fusion Product can be accessed at https://www.earthdata.nasa.gov/. Aboveground biomass data are available from https://dx.doi.org/10.5285/95913ffb6467447ca72c4e9d8cf30501. Forest Intactness data are available at www.forestlandscapeintegrity.com. Forest management data are available from https://doi.org/10.5281/zenodo.5879022. Biodiversity Intactness data are available at https://gee-community-catalog.org/projects/bii/. Natural and modified forest habitats are available from UN Environment Programme World Conservation Monitoring at https://data-gis.unep-wcmc.org/portal/home/index.html. The protected areas data can be accessed at https://www.resdc.cn/ and www.protectedplanet.net. Data on primary forests, plantation polygons, forest loss and forest gain are obtained from Global Forest Watch at https://www.globalforestwatch.org/.

Code availability

The basic code framework for the tree mapping is available under

https://github.com/sizhuoli/TreeCountSegHeight.

References

1. Pan, Y., Birdsey, R. A., Phillips, O. L., Houghton, R. A., Fang, J., Kauppi, P. E., ... & Murdiyarso, D. (2024). The enduring world forest carbon sink. Nature, 631(8021), 563-569.
2. Felipe-Lucia, M. R., Soliveres, S., Penone, C., Manning, P., van der Plas, F., Boch, S., ... & Allan, E. (2018). Multiple forest attributes underpin the supply of multiple ecosystem services. Nature Communications, 9(1), 4839.
3. McDowell, N. G., Allen, C. D., Anderson-Teixeira, K., Aukema, B. H., Bond-Lamberty, B., Chini, L., ... & Xu, C. (2020). Pervasive shifts in forest dynamics in a changing world. Science, 368(6494), eaaz9463.
4. Feng, Y., Ziegler, A. D., Elsen, P. R., Liu, Y., He, X., Spracklen, D. V., ... & Zeng, Z. (2021). Upward expansion and acceleration of forest clearance in the mountains of Southeast Asia. Nature Sustainability, 4(10), 892-899.
5. Chen, C., Park, T., Wang, X., Piao, S., Xu, B., Chaturvedi, R. K., ... & Myneni, R. B. (2019). China and India lead in greening of the world through land-use management. Nature Sustainability, 2(2), 122-129.
6. Zhang, X., Wan, W., & Estoque, R. C. (2025). Impacts of urban and cropland expansions on natural habitats in Southeast Asia. Nature Communications, 16(1), 8479.
7. Tong, X., Brandt, M., Yue, Y., Zhang, X., Fensholt, R., Ciais, P., ... & Jepsen, M. R. (2023). Reforestation policies around 2000 in southern China led to forest densification and expansion in the 2010s. Communications Earth & Environment, 4(1), 260.
8. Global forest resources assessments, FRA 2025 country reports. (FAO)
9. Peng, D., Zhang, B., Zheng, S., Ju, W., Chen, J. M., Ciais, P., ... & Zhang, X. (2025). Newly established forests dominated global carbon sequestration change induced by land cover conversions. Nature Communications, 16(1), 6570.
10. Jose, J. K. (2024). India’s tree-planting strategies fall short. Science, 385(6711), 836-837.
11. Gamfeldt, L., Snäll, T., Bagchi, R., Jonsson, M., Gustafsson, L., Kjellander, P., ... & Bengtsson, J. (2013). Higher levels of multiple ecosystem services are found in forests with more tree species. Nature Communications, 4(1), 1340.
12. Guillaume, T., Kotowska, M. M., Hertel, D., Knohl, A., Krashevska, V., Murtilaksono, K., ... & Kuzyakov, Y. (2018). Carbon costs and benefits of Indonesian rainforest conversion to plantations. Nature Communications, 9(1), 2388.
13. Wang, C., Zhang, W., Li, X., & Wu, J. (2022). A global meta-analysis of the impacts of tree plantations on biodiversity. Global Ecology and Biogeography, 31(3), 576-587.
14. Brandt, M., Chave, J., Li, S., Fensholt, R., Ciais, P., Wigneron, J. P., ... & Igel, C. (2025). High-resolution sensors and deep learning models for tree resource monitoring. Nature Reviews Electrical Engineering, 2(1), 13-26.
15. Lang, N., Jetz, W., Schindler, K., & Wegner, J. D. (2023). A high-resolution canopy height model of the Earth. Nature Ecology & Evolution, 7(11), 1778-1789.
16. Liu, S., Brandt, M., Nord-Larsen, T., Chave, J., Reiner, F., Lang, N., ... & Fensholt, R. (2023). The overlooked contribution of trees outside forests to tree cover and woody biomass across Europe. Science Advances, 9(37), eadh4097.

17. Fagan, M. E., Kim, D. H., Settle, W., Ferry, L., Drew, J., Carlson, H., ... & Ordway, E. M. (2022). The expansion of tree plantations across tropical biomes. Nature Sustainability, 5(8), 681-688.
18. Scheeres, J., de Jong, J., Brede, B., Brancalion, P. H., Broadbent, E. N., Zambrano, A. M. A., ... & de Almeida, D. R. A. (2023). Distinguishing forest types in restored tropical landscapes with UAV-borne LIDAR. Remote Sensing of Environment, 290, 113533.
19. Feng, Y., Schmid, B., Loreau, M., Forrester, D. I., Fei, S., Zhu, J., ... & Fang, J. (2022). Multispecies forest plantations outyield monocultures across a broad range of conditions. Science, 376(6595), 865-868.
20. Gao, X., Reich, P. B., Vincent, J. R., Fagan, M. E., Chazdon, R. L., Fritz, S., ... & Wang, D. (2025). The importance of distinguishing between natural and managed tree cover gains in the moist tropics. Nature Communications, 16(1), 6092.
21. Clough, Y., Krishna, V. V., Corre, M. D., Darras, K., Denmead, L. H., Meijide, A., ... & Scheu, S. (2016). Land-use choices follow profitability at the expense of ecological functions in Indonesian smallholder landscapes. Nature Communications, 7(1), 13137.
22. Danylo, O., Pirker, J., Lemoine, G., Ceccherini, G., See, L., McCallum, I., ... & Fritz, S. (2021). A map of the extent and year of detection of oil palm plantations in Indonesia, Malaysia and Thailand. Scientific data, 8(1), 96.
23. Jiang, Y., & Neumann, M. (2025, August). Not every tree is a forest: Benchmarking forest types from satellite remote sensing. In IGARSS 2025-2025 IEEE International Geoscience and Remote Sensing Symposium (pp. 808-813). IEEE.
24. Gosling, J., Jones, M. I., Arnell, A., Watson, J. E., Venter, O., Baquero, A. C., & Burgess, N. D. (2020). A global mapping template for natural and modified habitat across terrestrial Earth. Biological Conservation, 250, 108674.
25. Simões, L. H., Guillemot, J., Ronquim, C. C., Weidlich, E. W., Muys, B., Fuza, M. S., ... & Brancalion, P. H. (2024). Green deserts, but not always: A global synthesis of native woody species regeneration under tropical tree monocultures. Global Change Biology, 30(4), e17269.
26. LaRue, E. A., Hardiman, B. S., Elliott, J. M., & Fei, S. (2019). Structural diversity as a predictor of ecosystem function. Environmental Research Letters, 14(11), 114011.
27. Ehbrecht, M., Schall, P., Ammer, C., & Seidel, D. (2017). Quantifying stand structural complexity and its relationship with forest management, tree species diversity and microclimate. Agricultural and forest meteorology, 242, 1-9.
28. de Conto, T., Armston, J., & Dubayah, R. (2024). Characterizing the structural complexity of the Earth's forests with spaceborne lidar. Nature Communications, 15(1), 8116.
29. Zhang, W., Xi, Y., Brandt, M., Ren, C., Bai, J., Ma, Q., & Fensholt, R. (2024). Stand structure of tropical forests is strongly associated with primary productivity. Communications Earth & Environment, 5(1), 796.
30. de Conto, T., Armston, J., & Dubayah, R. (2026). Scalable deep fusion of spaceborne lidar and synthetic aperture radar for global forest structural complexity mapping. Machine Learning: Earth, 2(1), 015002.
31. Shaw, D.C. (2004) Vertical organization of canopy biota. In: Forest canopies. Amsterdam: Elsevier, pp. 73–101.
32. Goetz, S., Steinberg, D., Dubayah, R. & Blair, B. (2007) Laser remote sensing of canopy habitat heterogeneity as a predictor of bird species richness in an eastern

temperate forest, USA. Remote Sensing of Environment, 108(3), 254–263.
33. Sverdrup-Thygeson, A., Ørka, H. O., Gobakken, T., & Naesset, E. (2016). Can airborne laser scanning assist in mapping and monitoring natural forests?. Forest Ecology and Management, 369, 116-125.
34. Liu, X., Feng, Y., Hu, T., Luo, Y., Zhao, X., Wu, J., ... & Su, Y. (2024). Enhancing ecosystem productivity and stability with increasing canopy structural complexity in global forests. Science Advances, 10(20), eadl1947.
35. Xu, X., Brandt, M., Tong, X., Mugabowindekwe, M., Yue, Y., Li, S., ... & Fensholt, R. (2026). Large-scale characterization of horizontal forest structure from remote sensing optical images. Remote Sensing in Ecology and Conservation.
36. Li, L., Liu, L., Yu, Z., Peñuelas, J., Sardans, J., Chen, Q., ... & Zhou, G. (2022). Carbon, nitrogen and phosphorus stoichiometry in natural and plantation forests in China. Forests, 13(5), 755.
37. Haase, P. (1995). Spatial pattern analysis in ecology based on Ripley's K-function: Introduction and methods of edge correction. Journal of vegetation science, 6(4), 575-582.
38. Ripley, B. D. (1976). The second-order analysis of stationary point processes. Journal of applied probability, 13(2), 255-266.
39. Moeur, M. (1993). Characterizing spatial patterns of trees using stem-mapped data. Forest science, 39(4), 756-775.
40. Santoro, M.; Cartus, O. (2025): ESA Biomass Climate Change Initiative (Biomass_cci): Global datasets of forest above-ground biomass for the years 2007, 2010, 2015, 2016, 2017, 2018, 2019, 2020, 2021 and 2022, v6.0. NERC EDS Centre for Environmental Data Analysis, 17 April 2025. doi:10.5285/95913ffb6467447ca72c4e9d8cf30501.
41. Grantham, H. S., Duncan, A., Evans, T. D., Jones, K. R., Beyer, H. L., Schuster, R., ... & Watson, J. E. M. (2020). Anthropogenic modification of forests means only 40% of remaining forests have high ecosystem integrity. Nature communications, 11(1), 5978.
42. Hudson, Lawrence N., Tim Newbold, Sara Contu, Samantha LL Hill, Igor Lysenko, Adriana De Palma, Helen RP Phillips et al. "The database of the PREDICTS (projecting responses of ecological diversity in changing terrestrial systems) project." Ecology and evolution 7, no. 1 (2017): 145-188.
43. Crowther, T. W., Glick, H. B., Covey, K. R., Bettigole, C., Maynard, D. S., Thomas, S. M., ... & Bradford, M. A. (2015). Mapping tree density at a global scale. Nature, 525(7568), 201-205.
44. Lesiv, M., Schepaschenko, D., Buchhorn, M., See, L., Dürauer, M., Georgieva, I., ... & Fritz, S. (2022). Global forest management data for 2015 at a 100 m resolution. Scientific Data, 9(1), 199.
45. Turubanova, S., Potapov, P.V., Tyukavina, A. and Hansen, M.C., 2018. Ongoing primary forest loss in Brazil, Democratic Republic of the Congo, and Indonesia. Environmental Research Letters, 13(7), p.074028. Accessed through Global Forest Watch on 09/12/2026. www.globalforestwatch.org.
46. Richter, J., Goldman, E., Harris, N., Gibbs, D., Rose, M., Peyer, S., Richardson, S., and H. Velappan. 2024. “Spatial Database of Planted Trees (SDPT Version 2.0).” Accessed through Global Forest Watch on 09/12/2026. www.globalforestwatch.org.
47. FRA 2025 Country Reports, Global Forest Resources Assessments.
48. Hansen et al., 2013. “High-Resolution Global Maps of 21st-Century Forest Cover Change.”. Accessed through Global Forest Watch on 09/12/2025.

www.globalforestwatch.org.
49. Potapov, P., Hansen, M. C., Pickens, A., Hernandez-Serna, A., Tyukavina, A., Turubanova, S., ... & Kommareddy, A. (2022). The global 2000-2020 land cover and land use change dataset derived from the Landsat archive: first results. Frontiers in Remote Sensing, 3, 856903.
50. Xu, Y., Yu, L., Ciais, P., Li, W., Santoro, M., Yang, H., & Gong, P. (2022). Recent expansion of oil palm plantations into carbon-rich forests. Nature Sustainability, 5(7), 574-577.
51. Hua, F., Wang, L., Fisher, B., Zheng, X., Wang, X., Yu, D. W., ... & Wilcove, D. S. (2018). Tree plantations displacing native forests: The nature and drivers of apparent forest recovery on former croplands in Southwestern China from 2000 to 2015. Biological Conservation, 222, 113-124.
52. Tessier, J. T., & Raynal, D. J. (2003). Use of nitrogen to phosphorus ratios in plant tissue as an indicator of nutrient limitation and nitrogen saturation. Journal of Applied Ecology, 40(3), 523-534.
53. Powae, G. M., & Rao, B. R. (2024). Quantification of soil nutrient stocks and stoichiometric ratios in Eucalyptus pellita biomass plantation chronosequence in Papua New Guinea. Catena, 247, 108564.
54. Liao, C., Luo, Y., Fang, C., Chen, J., & Li, B. (2012). The effects of plantation practice on soil properties based on the comparison between natural and planted forests: a meta-analysis. Global ecology and biogeography, 21(3), 318-327.
55. Bosela, M., Marcis, P., Polťák, D., Rybár, J., Fleischer Sr, P., Fleischer Jr, P., ... & Mäkipää, R. (2025). Norway spruce monoculture has lower resilience and carbon sequestration capacity than a more diverse broadleaved forest: A case study in Central Europe. Forest Ecology and Management, 591, 122829.
56. Lelli, C., Bruun, H. H., Chiarucci, A., Donati, D., Frascaroli, F., Fritz, Ö., ... & Heilmann-Clausen, J. (2019). Biodiversity response to forest structure and management: Comparing species richness, conservation relevant species and functional diversity as metrics in forest conservation. Forest Ecology and Management, 432, 707-717.
57. Barabás, G. (2021). Biodiversity and community structure. Proceedings of the National Academy of Sciences, 118(11), e2101176118.
58. Delgado-Baquerizo, M., Maestre, F. T., Reich, P. B., Jeffries, T. C., Gaitan, J. J., Encinar, D., ... & Singh, B. K. (2016). Microbial diversity drives multifunctionality in terrestrial ecosystems. Nature communications, 7(1), 10541.
59. Sinclair, J. S., Welti, E. A., Altermatt, F., Álvarez-Cabria, M., Aroviita, J., Baker, N. J., ... & Haase, P. (2024). Multi-decadal improvements in the ecological quality of European rivers are not consistently reflected in biodiversity metrics. Nature ecology & evolution, 8(3), 430-441.
60. Pereira, H. M., Ferrier, S., Walters, M., Geller, G. N., Jongman, R. H., Scholes, R. J., ... & Wegmann, M. (2013). Essential biodiversity variables. Science, 339(6117), 277-278.
61. Sun, T., Hughes, A. C., He, K., & Yu, L. (2026). Ecological Integrity Index, timely annual tracking of biodiversity change. Scientific Data.
62. Bae, S., Levick, S. R., Heidrich, L., Magdon, P., Leutner, B. F., Wöllauer, S., ... & Müller, J. (2019). Radar vision in the mapping of forest biodiversity from space. Nature Communications, 10(1), 4757.
63. Marconcini, M., Metz-Marconcini, A., Üreyen, S., Palacios-Lopez, D., Hanke, W.,

Bachofer, F., ... & Strano, E. (2020). Outlining where humans live, the World Settlement Footprint 2015. Scientific Data, 7(1), 242.
64. Tong, X., Xu, Q., Yue, Y., Wang, K., Du, H., Fensholt, R., Li, S., Xu, X., Bai, Y., Yang, X., et al. (2025). Old-Growth Forest Patches Are Widespread Outside Nature Reserves in Southern China. https://doi.org/10.21203/rs.3.rs-7643250/v1
65. Reiner, F., Brandt, M., Tong, X., Skole, D., Kariryaa, A., Ciais, P., ... & Fensholt, R. (2023). More than one quarter of Africa's tree cover is found outside areas previously classified as forest. Nature Communications, 14(1), 2258.
66. Brandt, M., Gominski, D., Reiner, F., Kariryaa, A., Guthula, V. B., Ciais, P., ... & Fensholt, R. (2024). Severe decline in large farmland trees in India over the past decade. Nature Sustainability, 7(7), 860-868.
67. Brandt, M., Tucker, C. J., Kariryaa, A., Rasmussen, K., Abel, C., Small, J., ... & Fensholt, R. (2020). An unexpectedly large count of trees in the West African Sahara and Sahel. Nature, 587(7832), 78-82.
68. Mugabowindekwe, M., Brandt, M., Chave, J., Reiner, F., Skole, D. L., Kariryaa, A., ... & Fensholt, R. (2023). Nation-wide mapping of tree-level aboveground carbon stocks in Rwanda. Nature Climate Change, 13(1), 91-97.
69. Tucker, C., Brandt, M., Hiernaux, P., Kariryaa, A., Rasmussen, K., Small, J., ... & Fensholt, R. (2023). Sub-continental-scale carbon stocks of individual trees in African drylands. Nature, 615(7950), 80-86.
70. Salehi, S.S.M., Erdogmus, D., Gholipour, A. (2017). Tversky Loss Function for Image Segmentation Using 3D Fully Convolutional Deep Networks. In: Wang, Q., Shi, Y., Suk, HI., Suzuki, K. (eds) Machine Learning in Medical Imaging. MLMI 2017. Lecture Notes in Computer Science, vol 10541. Springer, Cham. https://doi.org/10.1007/978-3-319-67389-9_44
71. Hämäläinen, A., Runnel, K., Ranius, T., & Strengbom, J. (2024). Diversity of forest structures important for biodiversity is determined by the combined effects of productivity, stand age, and management. Ambio, 53(5), 718-729.
72. Ehbrecht, M., Seidel, D., Annighöfer, P., Kreft, H., Köhler, M., Zemp, D. C., ... & Ammer, C. (2021). Global patterns and climatic controls of forest structural complexity. Nature communications, 12(1), 519.
73. Hui, G., Zhang, G., Zhao, Z., & Yang, A. (2019). Methods of forest structure research: A review. Current Forestry Reports, 5(3), 142-154.
74. McElhinny, C., Gibbons, P., Brack, C., & Bauhus, J. (2005). Forest and woodland stand structural complexity: its definition and measurement. Forest Ecology and Management, 218(1-3), 1-24.
75. Hiernaux, P., Issoufou, H. B. A., Igel, C., Kariryaa, A., Kourouma, M., Chave, J., ... & Savadogo, P. (2023). Allometric equations to estimate the dry mass of Sahel woody plants mapped with very-high resolution satellite imagery. Forest Ecology and Management, 529, 120653.
76. Li, S., Brandt, M., Tong, X., Oehmcke, S., Igel, C., Gieseke, F., ... & Ciais, P. (2023). Deep learning tree and forest biomass from sub-meter resolution images. https://doi.org/10.21203/rs.3.rs-3335298/v1

Acknowledgments

This work was funded by the National Key Research and Development Program of China (grant agreement no. 2023YFF1305700), Bagui Scholars Program of Guangxi, the National Natural Science Foundation of China (grant agreement no. 42525104, W2412151, 42371129), the Danish National Research Foundation, Center for Remote Sensing and Deep Learning of Global Tree Resources (TreeSense; DNRF192), Combining LAnd-use, modeling and Remote-sensing to Transform carbon budgets (CLARiTy)

Author Contributions

XX, MB, XT, RF designed the study. DG, SL, FR, MM developed the code for the deep learning pipeline. JS, CI wrote the code for Ripley's K function. The Gaofen data were provided by ZC, YB. The first draft was written by MB and XX with support by RF, XT, JP, JC, CI, PC. All authors contributed to the final draft of the manuscript.

Competing interest

The authors declare no competing interests.

Extended Data

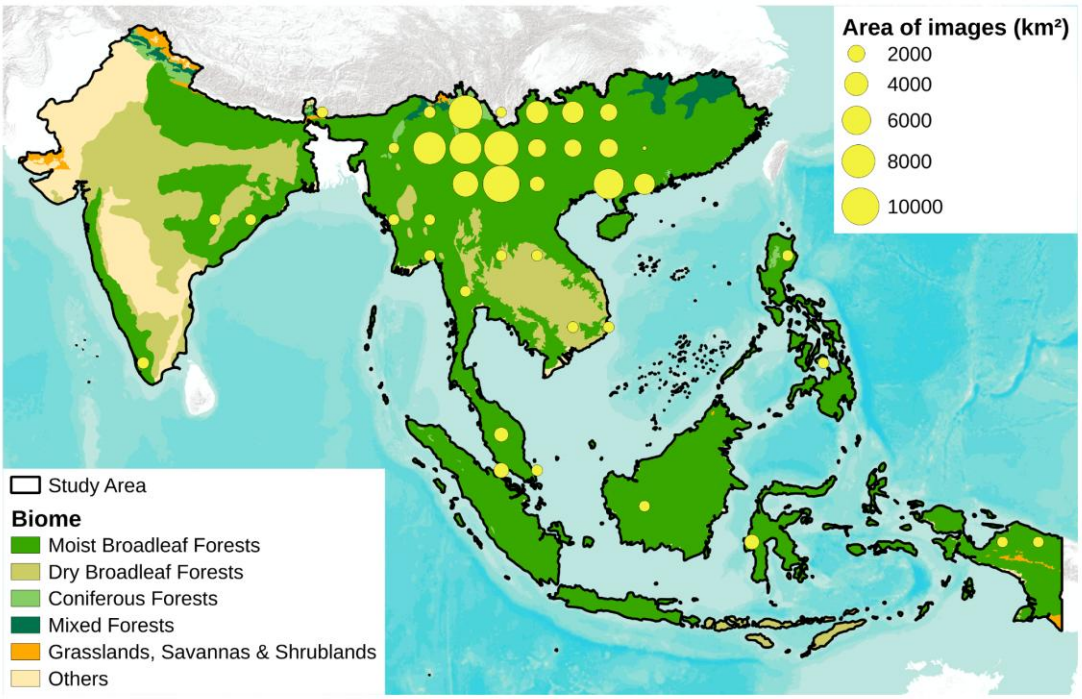

Extended Data Fig. 1: Study area and distribution of Gaofen images used for tree segmentation, aggregated into 2.5° × 2.5° grids. Biomes are aggregated into 6 classes: Moist Broadleaf Forests includes “Tropical & Subtropical Moist Broadleaf Forests”; Dry Broadleaf Forests includes “Tropical & Subtropical Dry Broadleaf Forests”; Coniferous Forests includes “Tropical & Subtropical Coniferous Forests” and “Temperate Conifer Forests”; Mixed Forests includes “Temperate Broadleaf & Mixed Forests”;Grasslands, Savannas & Shrublands includes “Tropical & Subtropical Grasslands, Savannas, & Shrublands”, “Flooded Grasslands & Savannas”, “Montane Grasslands & Shrublands”; Others includes “Tundra”, “Deserts & Xeric Shrublands” and “Mangroves”.

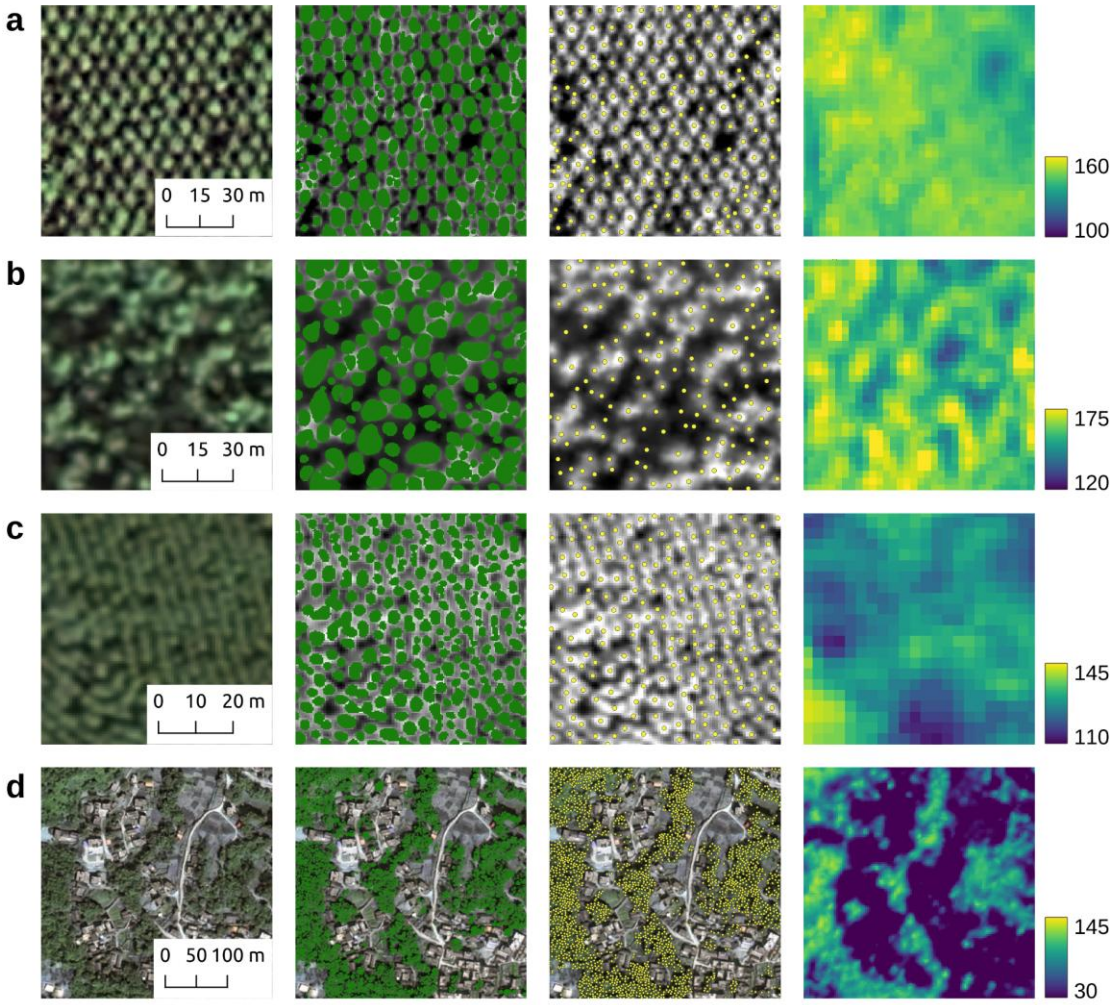

Extended Data Fig. 2: Examples of tree crown segmentation, tree location and tree probability. a, trees in palm plantation; b, trees in forest; c, trees in eucalyptus plantation; d trees in mixed landscape.

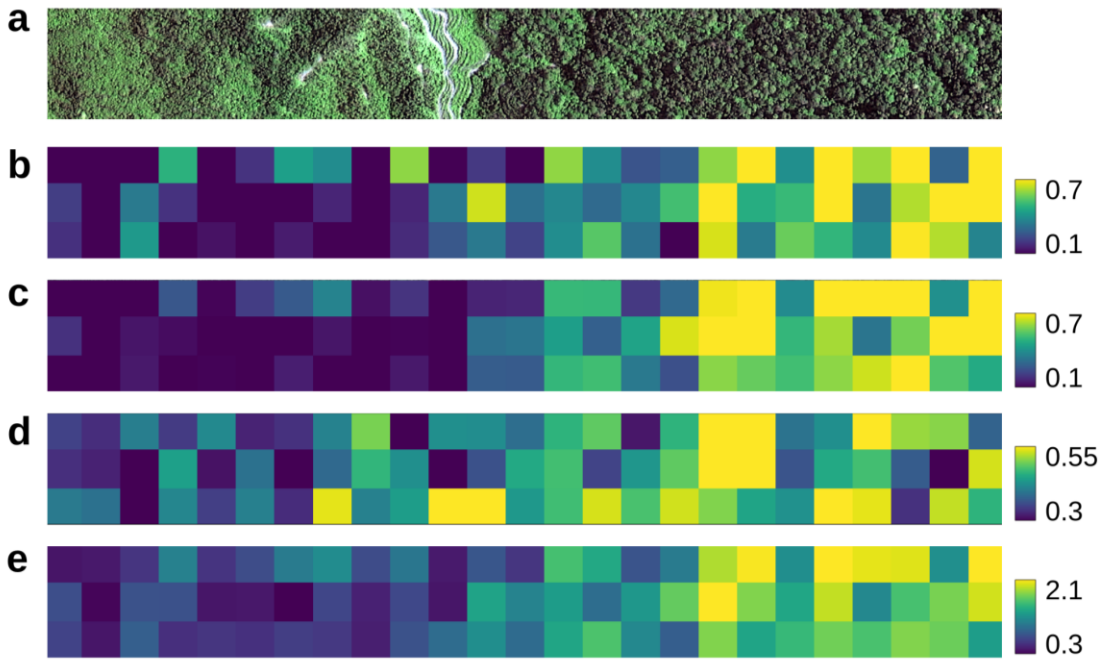

Extended Data Fig. 3: Examples of different structure metrics in this study and the horizontal structure index (HSI). a, GF-2 images; b, weighted standard deviation of crown size; c, coefficient of variation of crown size; d, Ripley's K index; e, horizontal structure index (HSI)

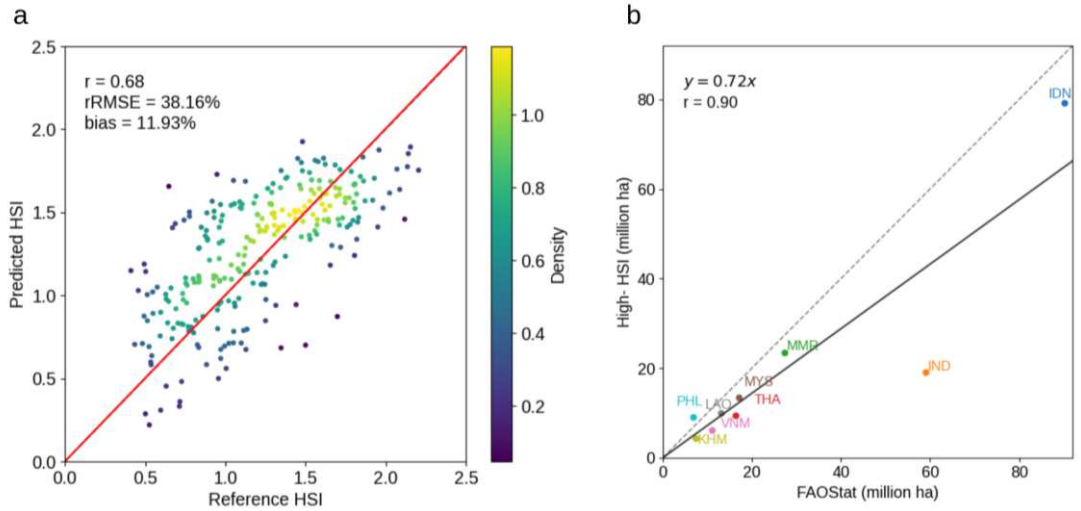

Extended Data Fig. 4: Horizontal structure index (HSI) model evaluation. a, Model predictions were evaluated using randomly selected grids that were excluded from the training dataset (n = 269). b, Comparison of the high HSI areas with naturally regenerating forests areas across different countries.

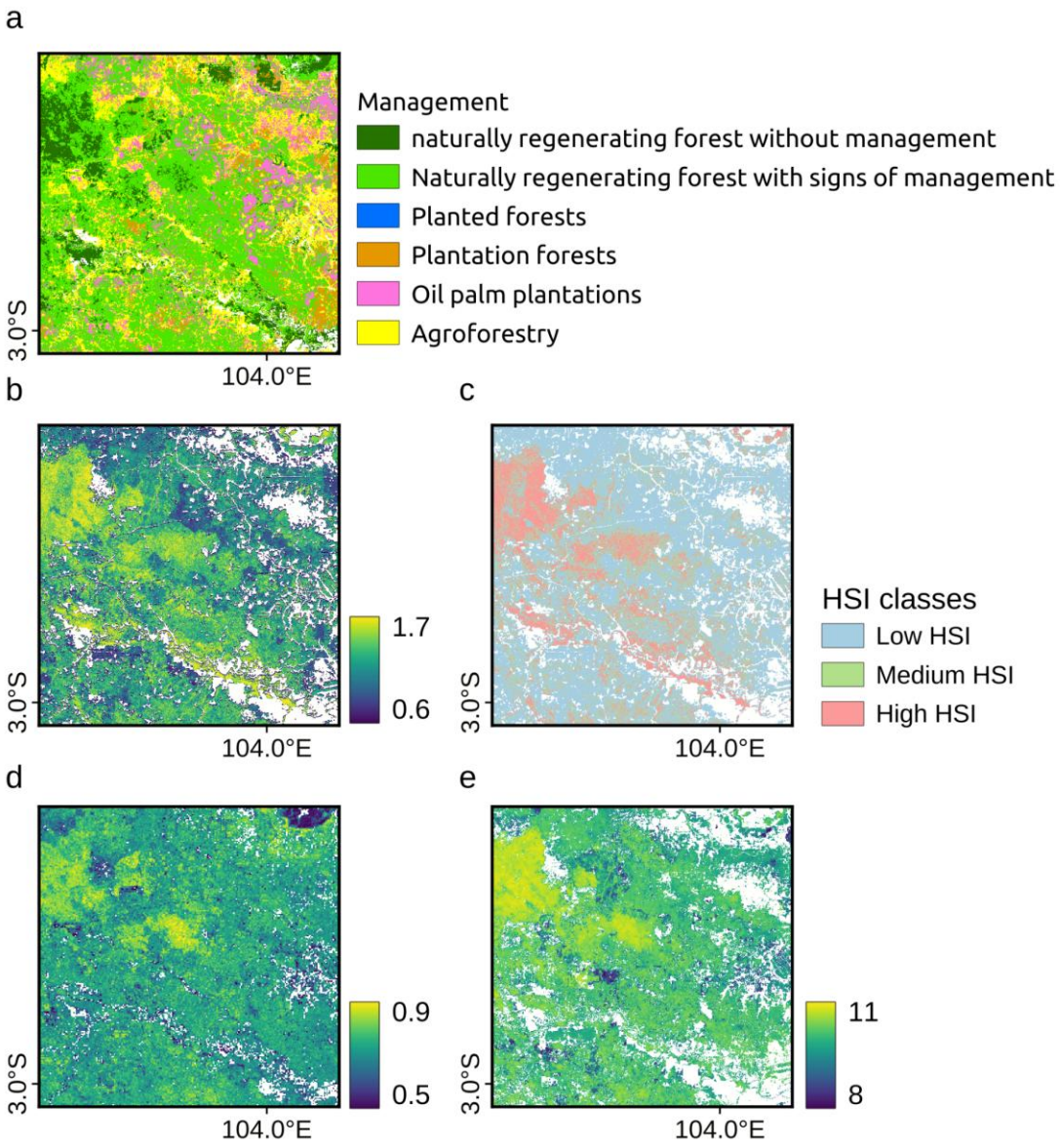

Extended Data Fig. 5: Visualization of forest management data and forest structure indices. a, forest management data [44]. b, horizontal forest structure complexity index (HSI). c, high-, medium-, and low-complexity forest structure. d, Stand structural indicator (SSI) index derived from GEDI [29]. e, Waveform Structural Complexity Index (WSCI) derived from GEDI[30] and masked using the tree cover dataset from this study.

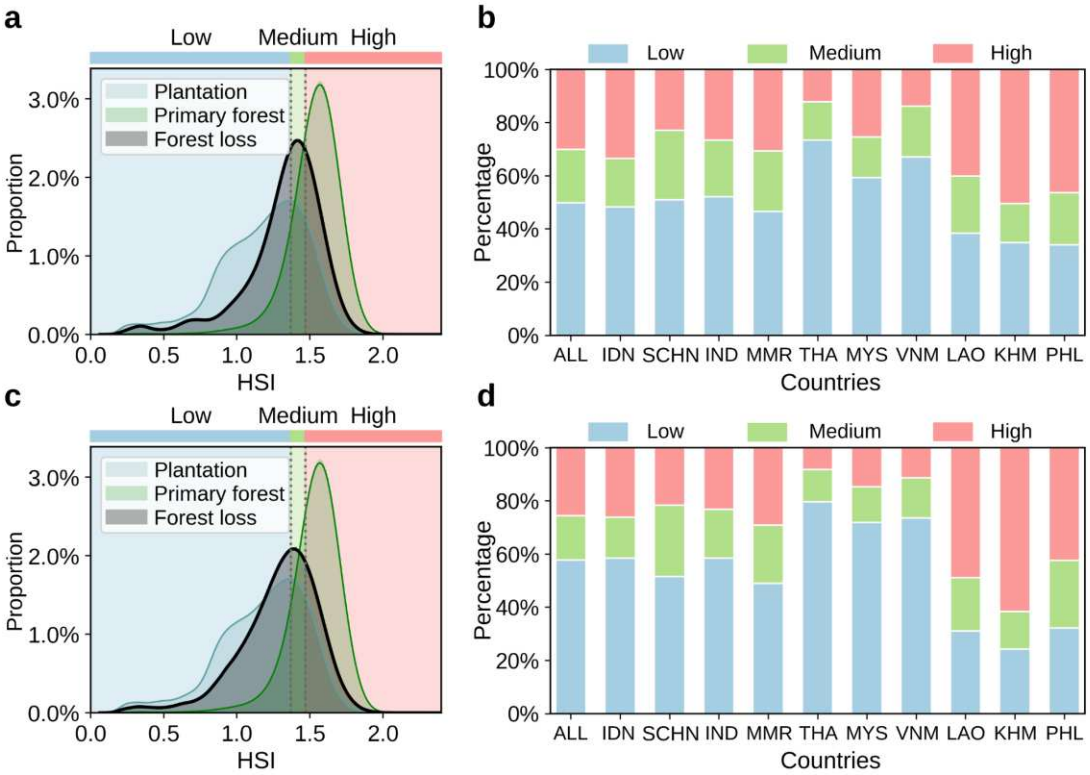

Extended Data Fig. 6: Horizontal forest structure complexity in forest loss areas exceeding 50% and 90% per grid. a, HSI distributions of forest loss exceeding 50% per grid overlaid by the distribution of HSI in primary forests and plantations for the study area. b, Proportions of high-, medium-, and low-complexity for forest loss exceeding 50% per grid in different countries in the study area. c, HSI distributions of forest loss exceeding 90% per grid overlaid by the distribution of HSI in primary forests and plantations for the study area. d, Proportions of high-, medium-, and low-complexity for forest loss exceeding 90% per grid in different countries in the study area.

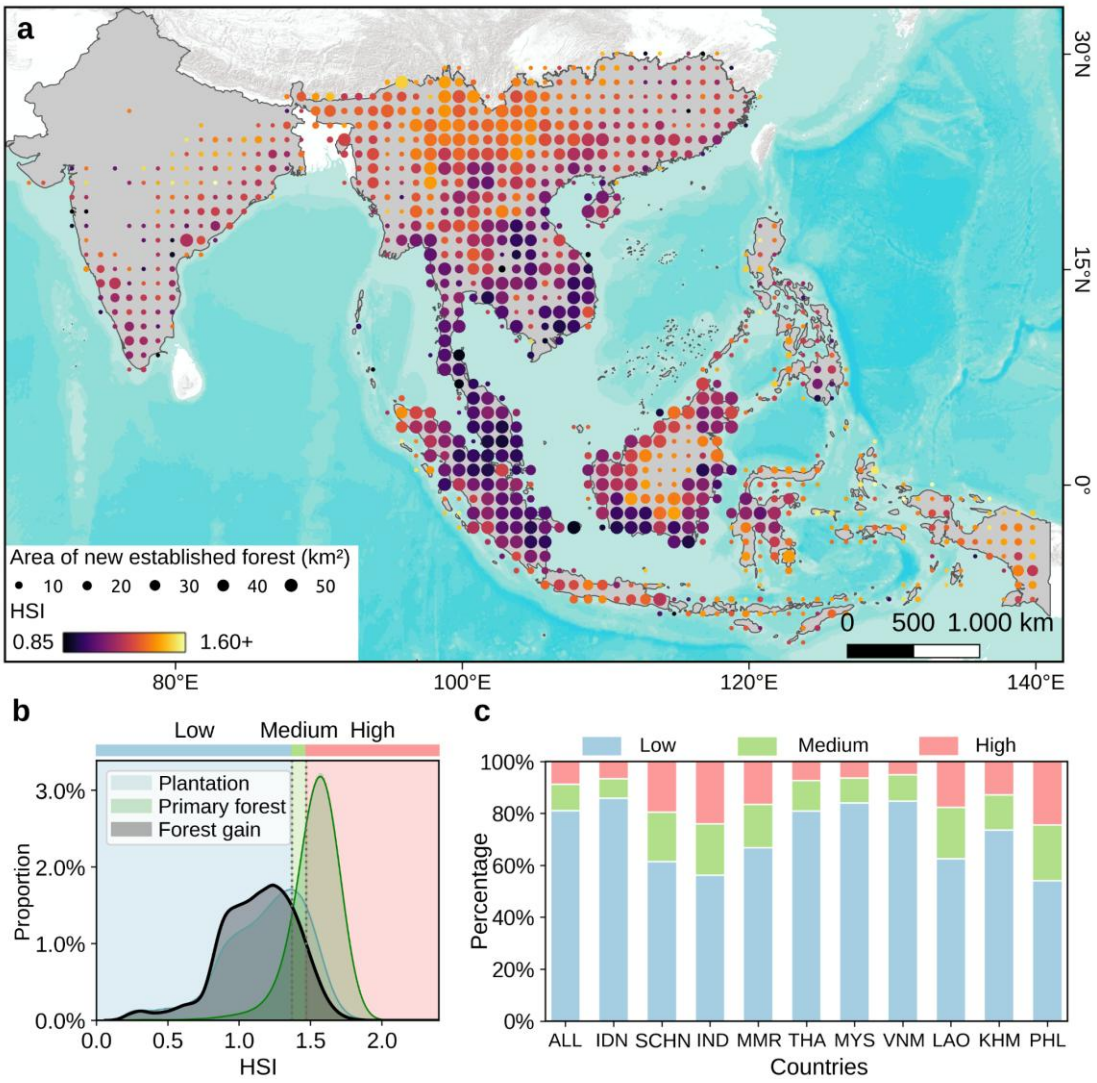

Extended Data Fig. 7: Structural complexity of forest gain during 2000-2020 based on forest gain data. a, Mean HSI and area of new forest for 1° by 1° grids. Circle color and circle size represents the mean HSI and the area of the new forest. b, HSI distributions of forest gain overlaid by the distribution of HSI in primary forests and plantations for the study area. c, Proportions of high-, medium-, and low-complexity for forest gain area in different countries in the study area.

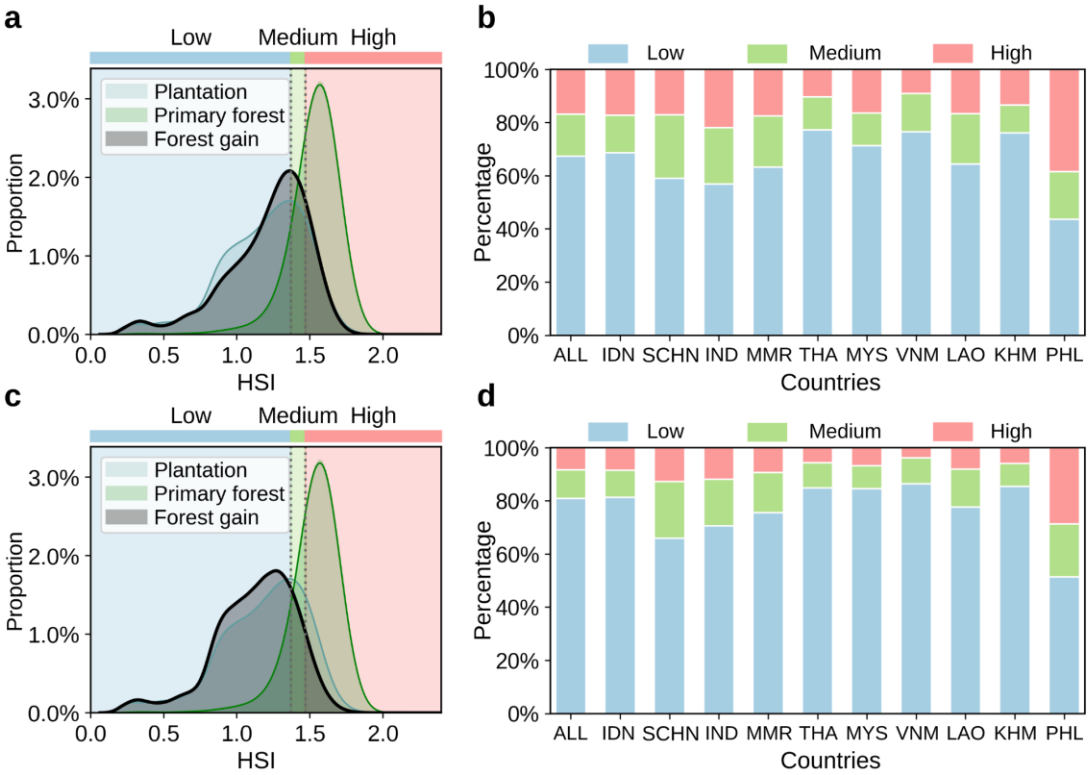

Extended Data Fig. 8: Horizontal forest structure complexity in new established forest areas exceeding 50% and 90% per grid. a, HSI distributions of new established forest areas exceeding 50% per grid overlaid by the distribution of HSI in primary forests and plantations for the study area. b, Proportions of high-, medium-, and low-complexity for new established forest areas exceeding 50% per grid in different countries in the study area. c, HSI distributions of new established forest areas exceeding 90% per grid overlaid by the distribution of HSI in primary forests and plantations for the study area. d, Proportions of high-, medium-, and low-complexity for new established forest areas exceeding 90% per grid in different countries in the study area.

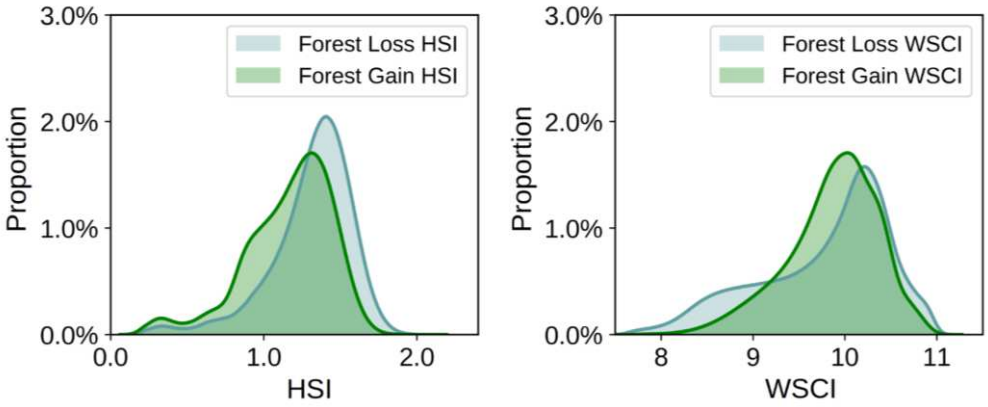

Extended Data Fig. 9: Distributions of HSI and WSCI in areas of forest loss and new established forest.

Extended Data Table 1. Forest area net change During 2000-2020

Countries	Forest area net change

	2000-2020 (1000ha)
Indonesia	3603.3
India	4718
Myanmar	-6324.2
Thailand	172.55
Malaysia	-506.65
Viet Nam	2893.15
Lao People's Democratic Republic	-837.4
Cambodia	-2904.2
Philippines	-82.8
Sum	731.75